Acceleration of acoustic aggregation of particles in acoustic levitation by collective effects. Application to cost-effective ultrasonic harvesting of microalgae

Ludovic Bellebon, Michael Levant, Mauricio Hoyos, Jean-Luc Aider

Acceleration of acoustic aggregation of particles in acoustic levitation by collective effects. Application to cost-effective ultrasonic harvesting of microalgae.

Ludovic Bellebon*
Laboratoire PMMH - UMR7636 CNRS - ESPCI Paris - PSL - Sorbonne Université, 7-9 quai Saint Bernard, 75005 Paris, France and Aenitis Technologies, Hôpital Saint-Louis, 1 avenue Claude Vellefaux, 75010 Paris, France

Michael Levant
TotalEnergies, PERL - Pôle d'Etudes et de Recherche de Lacq, 64170 Lacq, France

Mauricio Hoyos and Jean-Luc Aider†
Laboratoire PMMH - UMR7636 CNRS - ESPCI Paris - PSL - Sorbonne Université, 7-9 quai Saint Bernard, 75005 Paris, France
(Dated: November 21, 2024)

Acoustic aggregation of particles in acoustic levitation is a well-known phenomenon. However, it is only well described in the dilute regime, i.e. when particles do not interact with each other. In this study, we first demonstrate that the acoustic focusing speed can be significantly increased when dealing with particle aggregates. These results suggest that acoustic aggregation can be more efficient when dealing with relatively dense suspensions. This principle is successfully applied to microalgae suspensions. It is shown that microalgae harvesting can be accelerated without power increase using acoustically induced flocculation if the initial concentration is sufficiently high. This demonstrates that a cost-effective industrial process for acoustic microalgae harvesting is possible.

I. INTRODUCTION

Acoustophoresis is the ability to move and sort micro or nano-objects using ultrasonic standing waves. Typically, a piezoelectric source generates an acoustic standing wave in a resonant microcavity or microchannel. Pressure potentials arise that create the acoustic radiation force (ARF) that can move particles, cells or microalgae toward pressure nodes or antinodes based on their mechanical properties (size, density, compressibility). One of the many advantages of acoustophoresis is its ability to move objects without contact and without labeling, making it a very useful method for various applications. For example, as a non-intrusive non-contact method, this technique can be used to pattern neuronal cell layers in a hydrogel [1, 2] or to form and culture acoustically levitated cell spheroids [3–6].

Acoustophoresis can also promote mixing processes using acoustic streaming. Indeed, acoustic traveling waves interacting with sharp edges can create streaming leading to the mixing of fluids [7, 8]. Another application is droplet manipulation for controlled chemical reactions [9], droplets generation [10] or particle encapsulation [11]. Microbubbles can also be mentioned for sonoporation [12]. In this case, microbubbles interact with the membrane of a cell, making it porous, and deliver molecules and proteins inside the cell.

However, the main application of acoustofluidics, combined with microfluidics, is acoustic sorting processes applied to particles [13–16], nanoparticles [17, 18] or cells, such as blood lipids [19], mononuclear cells [20] or macrophages tagged by gas vesicles [21]. Cell washing is also relevant by using a collection buffer to remove white blood cells from the lysed blood and move them into PBS (Phosphate Buffered Saline) [22]. To achieve good efficiency, cells need to move as quickly as possible to the pressure nodes, which allows for increased flow rates and to handle the large volumes required by hospitals. This has been achieved recently [23] by removing albumin and collecting adipose-derived MSCs (Mesenchymal Stromal Cells) at high flow rates (up to 45 $mL.h^{-1}$).

The main phenomenon used in these various applications is the reaction of isolated particles or cells to ARF. This means that only dilute suspensions are considered and that the particles behave independently. In practice, in many industrial processes it is necessary to deal with relatively dense suspensions where particles can interact with each other when moved by ARF. In these cases, there is no clear theoretical framework describing acoustophoresis for dense suspensions and unexpected behaviors can appear, which can lead to new levers of manipulation. This is the reason it is important to study and analyze the collective effects, which can occur when manipulating particle aggregates using ARF and how to take advantage of these effects when manipulating microalgae.

Indeed, in addition to particle concentration, filtration and separation, acoustic aggregation has also been suggested as a non-destructive and low-energy method for microalgae harvesting. Microalgae have attracted great interest due to their numerous applications in the pharmaceutical [24], agri-food [25–27] and cosmetic [28, 29] fields, as well as in the energy sector, to produce biofuels

* ludovic.bellebon@orange.fr
† jean-luc.aider@espci.fr

[30], an important alternative to fossil fuels on the path to climate change mitigation. In a typical algal production process, algae harvesting is a key step required to increase the tailings concentrations to the values needed for an economically viable process [31]. Several methods are currently used for microalgae harvesting, such as filtration [32], flotation [33] or centrifugation [34, 35]. Others are under investigation, such as flocculation [36–39] or electrocoagulation [40], to name a few. None of these methods is optimal for algae harvesting, as they have different efficiencies, drawbacks and energy costs. When evaluating separation efficiency versus capital and operating costs, the choice should be made based on the overall process, algae type and final product value. Despite the advantages and ongoing research, scaling up is considered a major barrier to the industrial integration of ultrasonic harvesting and preference is given to lower-cost methods, especially for low-value-chain products.

In the first part of the paper, we will study the acoustic focusing of single particles and particle aggregates in a closed microcavity. We will investigate the influence of particle size and particle number in an aggregate on the acoustic focusing towards the leviation plane. In a second step, we will study the acoustic focusing of microalgae in the same acoustofluidic cavity. Finally, we will show in the last part of the paper that collective effects can significantly improve the energy efficiency of an acoustically assisted harvesting process in a static resonator, which could alleviate major barriers to scaling up and integration.

II. ACOUSTIC RADIATION FORCE

The acoustic radiation force (ARF) is a force exerted on objects in a fluid due to the interaction of sound waves with the object. This force arises when acoustic waves propagate through a medium, and their momentum is transferred to the object. It results from the scattering and absorption of sound waves by an object, creating a pressure differential across the object. The force can be caused by either standing or traveling sound waves. In traveling waves, the force typically pushes objects in the direction of wave propagation. In an acoustic standing wave (ASW), objects tend to move toward regions of low or high pressure (nodal or antinodal points).

In this study, only the case of an ASW created inside a resonant cavity will be considered. This cavity consists of two opposite walls, one transmitting the acoustic wave (emitter) emitted by a transducer, the other reflecting the acoustic wave (Fig. 1a). The resonance condition requires that the cavity height h be a multiple of half the acoustic wavelength λ_{ac} ($h = n\frac{\lambda_{ac}}{2}$). In this case, the particles suspended inside the cavity will be displaced towards the acoustic pressure node by the axial component of the ARF, as illustrated in Fig. 1b. Once in the acoustic pressure node (also called the acoustic levitation plane), the particles move radially toward the center of the cavity and form an aggregate that can be maintained in acoustic levitation as long as necessary.

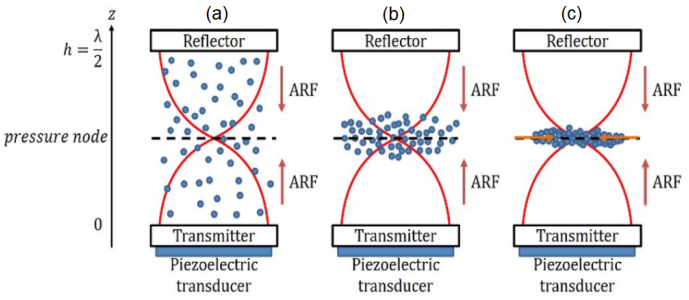

FIG. 1. Acoustic Radiation Force effect on a suspension scheme. a) ARF moves objects toward the focusing plane close to the nodal plane. b) Once in the focusing plane, particles aggregate in the center of the cavity due to the radial component of the ARF (c).

There are many different analytical expressions for the ARF, taking into account different physical hypothesis, either on the particles and / or the nature of the fluid. 90 years ago, King [41] derived the first expression for the ARF for incompressible particles in a plane acoustic wave and an inviscid fluid. Later, Yosioka and Kawasima calculated the ARF for compressible particles in plane acoustic waves [42]. Gor'Kov [43] generalized these works to arbitrary sound waves defining the ARF F_{rad} on a small particle as the gradient of an acoustic potential U^{rad}:

$$F_{rad} = -\nabla(U^{rad}). \tag{1}$$

It is then possible to derive the expression of the ARF by using the proper expression for the acoustic potential and taking into account a planar standing wave, as detailed by Bruus [44]. Later, Doinikov [45, 46] developed a more realistic description taking into account the viscosity and the thermal conductivity of the fluid. It results into two supplementary terms in the acoustic contrast factor (to be defined in the following). In our case, the supplementary terms are negligible compared to the original term obtained with an inviscid fluid. This is the reason why, in the following, we will use the expression proposed by Yosioka and Kawasima as a good approximation. The main hypothesis are that the particles are compressible and spherical, floating in a inviscid fluid and submitted to a plane acoustic wave. The diameter of the particles d_p has to be small compared to the acoustic wavelength, i.e. $d_p \ll \lambda_{ac}$ (Rayleigh regime). Using these hypothesis, one can derive the following expression for the ARF applied on an isolated particle:

$$\vec{F}_{rad} = \frac{\pi}{12} \langle E_{ac} \rangle \, k d_p^3 \phi sin(2kz) \vec{e_z}, \tag{2}$$

where $\langle E_{ac} \rangle$ is the acoustic energy density, k is the acoustic wave number ($k = \frac{2\pi}{\lambda_{ac}}$), ϕ is the acoustic contrast factor and z is the axial position of the particle.

The acoustic contrast factor ϕ quantifies the acoustic response of an object as a function of the difference between its mechanical properties and those of the surrounding fluid. It is defined as follows:

$$\phi = \frac{5\rho_p - 2\rho_f}{2\rho_p + \rho_f} - \frac{\beta_p}{\beta_f}, \tag{3}$$

with ρ_p and ρ_f the densities respectively of the particle and the medium, while β_p and β_f are respectively the compressibilities of the particle and of the medium. It is important to notice that if $\phi > 0$, the ARF is positive and the objects will move toward the pressure nodes. On the contrary, if $\phi < 0$ the objects will migrate toward the antinodes. In the following, the fluid medium will be water and the acoustic contrast factor of the particles or microalgae will be positive, leading to aggregation in the pressure nodes. The acoustic contrast factor of the polystyrene beads (in water) that will be used in the experiments can be calculated using Eq. 3. We obtain $\phi = 0.24$. Using Eq. 2, we can then estimate the acoustic force applied to a polystyrene beads. For a 10 μm diameter bead, and an acoustic energy density of 10 $J.m^{-3}$, the acoustic force is $F_{rad} = 2.10^{-12}$ N.

Once the particles have reached the acoustic levitation plane the axial component of the ARF vanishes, while the transverse component of the ARF F_T becomes maximum. In the levitation plane, the radial component of the ARF can be written as [47]:

$$\vec{F}_T = d_p^3 \frac{3(\rho_p - \rho_f)}{\rho_f + 2\rho_p} \vec{\nabla} \langle E_{ac} \rangle , \tag{4}$$

with $\vec{\nabla} \langle E_{ac} \rangle$ (x,y) the acoustic energy gradient in the levitation plane. The acoustic energy gradient is not known, but usually this component is 10 to 100 times weaker than the axial ARF. This component, which is negligible outside the levitation plane, induces the displacements of the particles toward the center of the cylindrical cavity where they form an aggregate (Fig. 1c). In the present study we focus on the axial displacements of the beads toward the levitation plane, so this component will not be further used or discussed.

Once the distance between the particles becomes small, they become attracted by each other because of the Bjerknes Force [48, 49]. More refined description taking into account interaction between particles either in a traveling or a standing plane [50] or even core-shell particles [51]. This short distance particle-particle attractive force plays a role to maintain the coherence of the aggregate after its formation in the acoustic levitation plane but also to favor the creation of small aggregates in the fluid when dealing with dense suspensions.

Using the fundamental principle of dynamics along the axial direction, it is possible to obtain an expression for the acoustic focusing velocity of an isolated particle, taking into account the axial component of the ARF (Eq. 2), the Stokes force and neglecting the buoyancy [52–54]. It gives the following expression for the acoustic focusing velocity $u_F(z)$ of a given particle:

$$u_F(z) = \frac{\langle E_{ac} \rangle \, k d_p^2 \phi}{36\mu} sin(2kz), \tag{5}$$

with μ the dynamic viscosity of the fluid. The axial velocity profile in the channel is maximal at $\frac{h}{4}$ and $\frac{3h}{4}$ while it is zero at the pressure node $\frac{h}{2}$ as well as at the channel walls (0 and h).

III. COLLECTIVE EFFECTS

The first indication of possible collective effects in acoustic focusing was based on an analogy with sedimentation. Indeed, it has been shown that the sedimentation of a group of particles is faster than that of a single particle. More precisely, Guazzelli [55] describes three sedimentation regimes. The first two are the cases of sedimentation of particles or fibers distributed homogeneously in a suspension. The third corresponds to the sedimentation of a particle cloud. It shows that a particle cloud undergoing sedimentation is affected by three distinct and cyclic phases:

- The first one is a spherical cloud. When it moves, particles at the periphery are ejected from the spheroid.
- In the second one the aggregate becomes longer in two directions giving it a flat shape. It no longer looses particles at the periphery.
- The third one is a break-up of the aggregate in at least two parts which take a spherical form behaving like the spherical clouds.

To quantify the transition from one regime to another, Huisman *et al.* [56] introduced a parameter called the Galileo number, which is defined as:

$$Ga = V_g \frac{D_n}{\nu}, \tag{6}$$

with V_g the sedimentation velocity, D_n the diameter of the cloud of particles and ν the fluid cinematic viscosity. Based on the Galileo number, Huisman *et al.* [56] found four main sedimentation regimes of sedimentation:

- a vertical sedimentation ($Ga \leq 155$),
- an inclined sedimentation ($155 \leq Ga \leq 185$),
- an instable oscillatory inclined sedimentation ($185 \leq Ga \leq 215$),
- a chaotic regime with $Ga \geq 215$.

Other studies have shown that the Galileo number also indicates when particles have a tendency to sediment like a column cluster [57, 58]. Using the Galileo number, it is possible to determine different sedimentation regimes of a particle and of a cluster of particles.

Because one could see the acoustic focusing of particles or aggregates toward the acoustic pressure node as an inverted sedimentation, we chose to characterize the different regimes using a similar non-dimensional number that can be associated to the transitions from one regime to another. This parameter is the acoustic focusing Reynolds number Re_{ac} and is written as:

$$Re_{ac} = V_{ag}\frac{D_{ag}}{\nu}, \tag{7}$$

with V_{ag} the aggregate acoustic focusing velocity and D_{ag} the aggregate diameter. These parameters can be measured experimentally, as will be shown in the following sections.

IV. MATERIALS AND METHODS

A. Resonant cavity

To study the acoustic focusing times required for particles or particle aggregates to reach the acoustic levitation plane, we used a cylindrical resonant cavity with a single acoustic node. It has a diameter $D = 25\ mm$ for a height $h = 330\ \mu$m, corresponding to a volume of 160 μL. The height of the cavity corresponds to the half-wavelength of the 2.24 MHz acoustic wave in water. The bottom of the cavity (transmitter) is made of a silicon wafer due to its flatness, the quality of its surface condition as well as the mirror effect which increases the contrast of the images when observed from the top of the cavity. The top of the cavity (reflector) is made of a quartz disk to allow observations from above using a microscope (Fig. 2a, b). A Signal Processing™ transducer is placed under the silicon disk (Fig. 2b). The side walls of the cavity are made of aluminum (Fig. 2c).

B. Experimental setup

A broadband ultrasonic transducer (Signal Processing™) is used to generate the 2.24 MHz acoustic wave. It is powered by a USB digital wave generator (TiePie™) that is monitored by a computer. The signal amplitude varies from 5 to 12 V. The cavity is placed on the motorized stage of an Olympus™ microscope. The transparency of the quartz cover allows easy observation of the cavity interior from above. A high-speed and high-sensitivity PCO™ Panda Bi camera is mounted on the microscope. It allows observations inside the cavity, which is illuminated by a CoolLed™ pe-4000 source (Fig. 2).

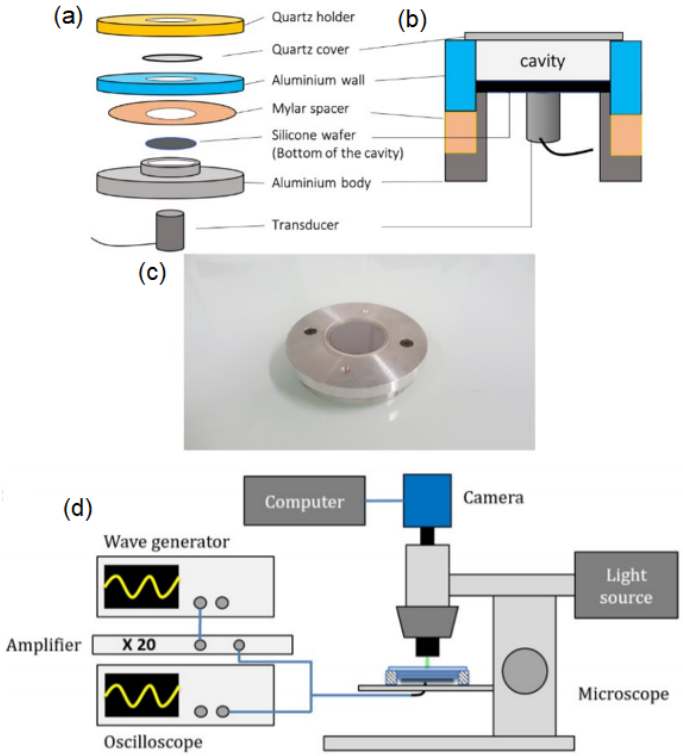

FIG. 2. Exploded view (a) and side view (b) of the cylindrical cavity used to study the motion of particles or cluster of particles induced by the ARF. Its diameter is 25 mm a height $h = 330\ \mu$m. c) Picture of the aluminum cavity. The drawings are not to scale. d) Sketch of the optic and acoustic setup. The cavity, coupled with the transducer, is placed on a motorized stage under a microscope. A signal generator is connected to the transducer to generate an acoustic wave, which is transmitted through the bottom of the cavity made of silicon. Observation and illumination are carried out through the quartz reflector at the top of the cavity (a). Axial and radial displacements of the particles can be monitored with a PCO™ Panda Bi camera plugged on the microscope [53].

Time series of snapshots of particles or microalgae are recorded on a computer.

C. Measurement of acoustic focusing time and velocity of aggregates

The observation axis z of the microscope is the same as the propagation axis of the acoustic wave that moves the particles or the aggregate towards the pressure node (Fig. 1). Therefore, we cannot directly measure the axial displacement of the particles. To measure the axial displacement of fluorescent particles, we can use the Airy ring or defocusing technique, by correlating the size of a particle's ring to its distance from the observation plane as described in [52, 53]. However, this technique is not well suited to the study of particle aggregates, which have various shapes (ellipsoids) and are composed of several particles. They create several superimposed Airy rings

that cannot be easily post-processed. Alternatively, the focusing time of the aggregate T_{foc-ag}, i.e. the time taken by an aggregate to reach the levitation plane, is measured. Knowing the distance to the levitation plane, we deduce the average acoustic focusing speed of the aggregate $V_{foc-ag} = \frac{h}{2T_{foc-ag}}$. Indeed, the initial position of the aggregate is at the bottom of the cavity before the activation of the acoustics, so that the distance to the levitation plane is $\frac{h}{2}$. In some cases, not all the particles composing the aggregate reach the focusing plane at the same time. In this case, we consider that the aggregate has reached the levitation plane when at least 90 % of its particles are visible inside the focusing plane. This is illustrated in Fig. 3 for an aggregate of 25 μm of polystyrene particles. It shows a time sequence showing an aggregate initially located at the bottom of the cavity (Fig. 3a) and successive snapshots once the acoustics are activated. After 200 ms, most of the particles have reached the levitation plane (Fig. 3f) and no clear difference is visible after 2 s (Fig. 3h).

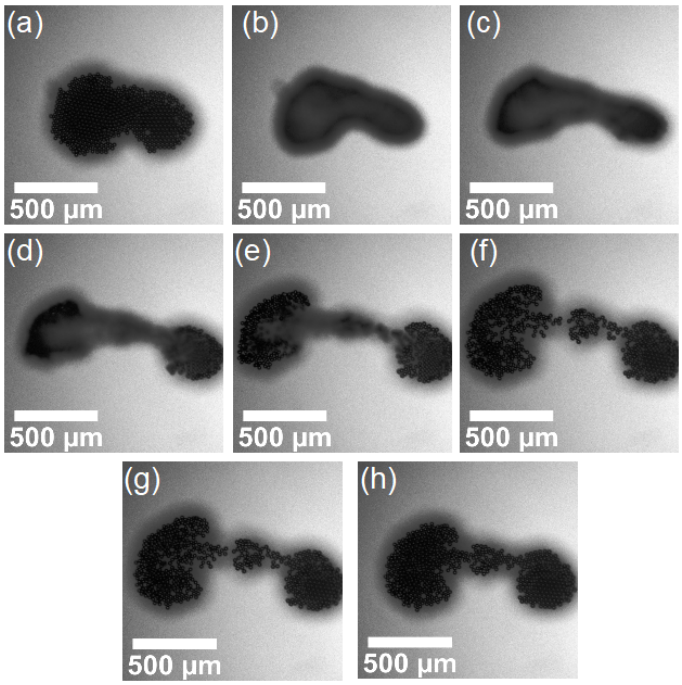

FIG. 3. Illustration of the axial displacement of an aggregate composed of 25 μm polystyrene particles during the acoustic focusing. Observations are made from the top of the cavity using a microscope. a) Picture showing a stable aggregate in the acoustic levitation plane, before sedimentation. b) When the acoustic is turned off, the aggregate sediments, reaching the bottom of the cavity. The picture is blurred because the focus is maintained in the middle of the cavity, in the levitation plane.

Then successive snapshots have been taken when acoustic is turned on: c) t=50 ms, d) t=100 ms, e) t=150 ms, f) t=200 ms, g) t=300 ms and h) t=2 s respectively. Movie on line.

D. Characterization of the aggregates

For this study, it is necessary to characterize particle aggregates through quantitative parameters. The first two obvious parameters are N_p, the number of particles and A_{ag} the total area of the aggregate measured in the snapshots taken when the aggregates are formed and stable in acoustic levitation. Indeed, aggregates of monodisperse particles spontaneously organize themselves into a 2D a quasi-crystalline lattice, as shown in Fig. 4. From this area, an equivalent diameter D_{ag} of the aggregate is defined by averaging the major and minor axis of the aggregate. Of course, it is associated with d_p the particle diameter.

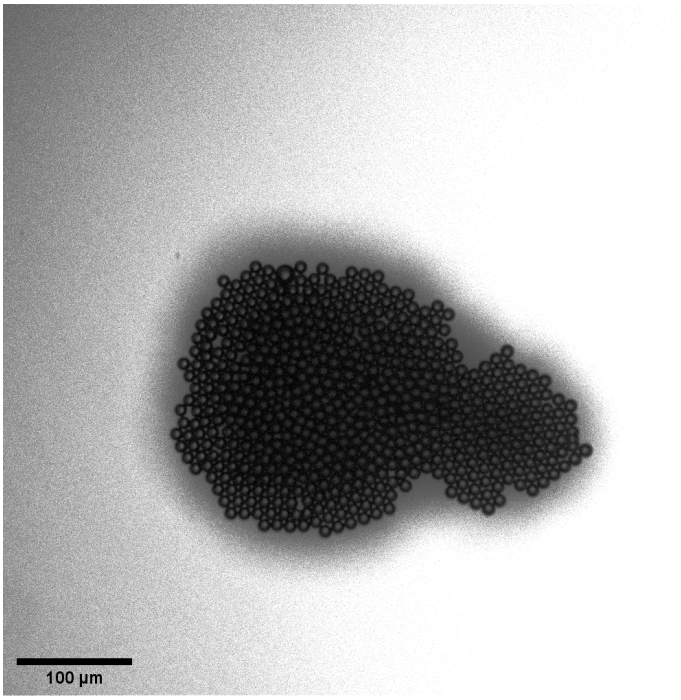

FIG. 4. Snapshot of an aggregate of 10 μm polystyrene particles in acoustic levitation. Once formed, the aggregate remain stable and can be quantified.

Since these are aggregates of particles, the porosity of the aggregates φ must be taken into account. It is defined as:

$$\varphi = \frac{A_{pores}}{A_{ag}}, \tag{8}$$

with A_{pores} the surface area occupied by pores. A_{ag} can be measured by image processing using ImageJ software. To estimate A_{pores} two steps are necessary. First, the number of particles inside the aggregate must be counted. Then, the solid surface area of the aggregate A_{sol} can be calculated as follows:

$$A_{sol} = \pi(\frac{d_p}{2})^2 N_p. \tag{9}$$

Finally, A_{pores} is simply the difference between the total surface area of the aggregate A_{ag} and the solid surface area of the aggregate A_{sol} occupied by the particles:

$$A_{pores} = A_{ag} - A_{sol}. \tag{10}$$

All these parameters can influence the response of aggregates to ARF.

V. RESULTS AND DISCUSSION

A. Acoustic focusing of isolated particles

For low concentrations, the particles can be considered as isolated and do not interact with each other. In this case, they migrate towards the pressure node at velocities depending on the voltage and frequency imposed by the ARF. But if the local concentration is sufficiently increased, the particles can interact and thus change speed.

The maximum acoustic focusing velocity of polystyrene particles was measured as a function of the acoustic energy injected into the cavity. The result is shown in Fig. 5 for three particle sizes: 10 μm, 25 μm and 40 μm.

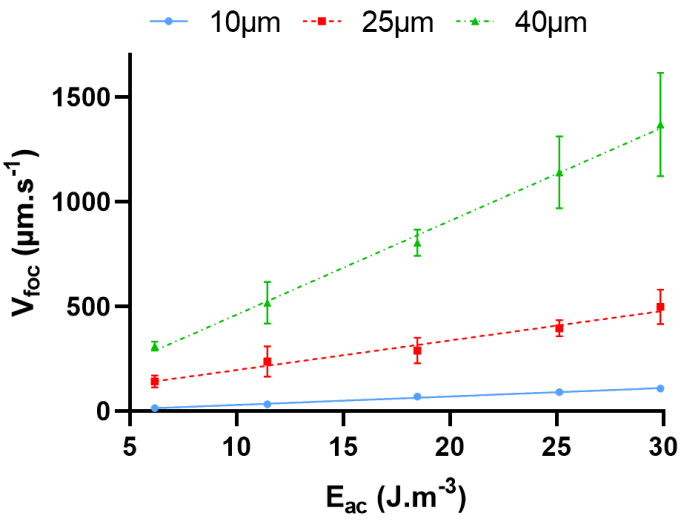

FIG. 5. Focusing velocity of isolated particles for 3 diameters (10, 25 and 40 μm) as a function of the acoustic energy density. Each point are averaged over 5 measurements. The lines are linear fits.

As expected and as described by the theory (Eq. 5), the focusing velocity depends linearly on the acoustic energy, which was measured using the defocusing technique presented in Dron and Aider [52]. It can also be seen that the larger the particle diameter, the higher the velocity. It should scale as d_p^2 (Eq. 5), which is approximately the case, considering the uncertainties in the particle size distribution.

B. Acoustic focusing of aggregates of particles

1. *Acceleration of the acoustic focusing of aggregate*

The Yosioka model, as most of the other models, describes only the acoustic force acting on an isolated spherical particle. Here we study the velocity induced by ARF on aggregates of polystyrene particles, which are mostly discoidal porous aggregates of arbitrary shape. This means that the Yosioka model (or any other model developed for a single isolated particle) is no longer valid.

To quantify the impact of collective effects on the focusing dynamics, the focusing velocities of aggregates was measured with different mean diameters ($D_{ag} =$ 42 μm to 585 μm) and composed of particles of a given diameter. Three different particle diameters were used to form the aggregates: 10 μm, 25 μm and 40 μm. In all cases, the focusing velocity of the isolated particles was also measured as a reference. The measurements were performed for increasing acoustic energy densities ranging from 5 $J.m^{-3}$ to 30 $J.m^{-3}$.

It is important to emphasize the difficulty associated with this type of experiments. Indeed, it is not possible to control a priori the number of particles inside an aggregate. The protocol then consisted in trying to create aggregates with a low concentration suspension of a given particle type. Low concentration suspensions were obtained by dilute high concentration of particles, bought to a supplier, with water. Due to the low number of particles present in the cavity, this was a difficult and time-consuming process. Once the aggregate was formed, the ultrasound was turned off and the aggregate was allowed to sediment. Then, the acoustics were turned on to monitor the movement of the aggregate towards the levitation plane. This explains the uncontrolled variations in the size of the aggregates. Nevertheless, it was sufficient to find a clear trend in the acoustic focusing towards the levitation plane.

The results obtained with the 10 μm particles are shown in Fig. 6. The first cluster has a diameter of 42 μm while the second has a diameter of 457 μm. The focusing velocities of the individual particle and the 42 μm diameter cluster are very close. The difference is insignificant compared to the 457 μm cluster. Its focusing velocity is much larger compared to the others, reaching more than 2 $mm.s^{-1}$ for 20 $J.m^{-3}$ and beyond. The focusing velocity increases drastically with the cluster diameter. We obtain an increase $\times 23$ of the focusing speeds between the aggregates of diameters 42 μm and 457 μm.

The results obtained with the 25 μm particles are shown in Fig. 7. The 60 μm diameter aggregate migrates slightly faster than the individual particle. The focusing velocities of the larger aggregates (192 μm and 502 μm diameter) increase considerably and reach up to 3.3 10^3 $\mu m.s^{-1}$ and 5 10^3 $\mu m.s^{-1}$ for 30 $J.m^{-3}$ respectively. In both cases, the increase in acoustic energy density leads to a quasi-linear increase in focusing velocities

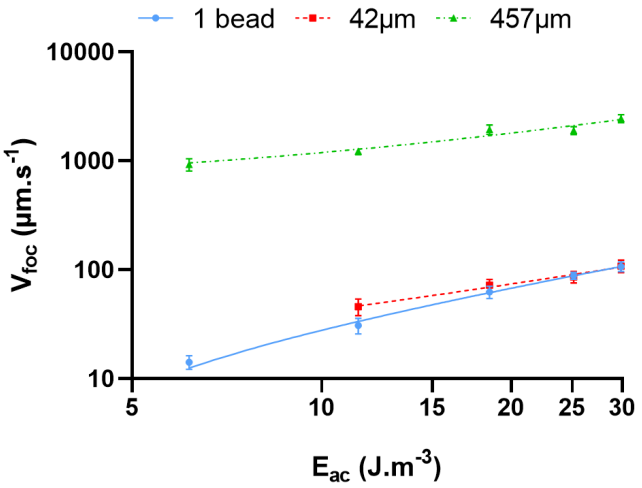

FIG. 6. Focusing velocities of $D_{ag} = 42$ μm and $D_{ag} = 457$ μm aggregates as a function of the acoustic energy. Aggregates are composed of only of 10 μm polystyrene particles. The focusing velocity of a single 10 μm polystyrene particle is added for comparison. The lines are linear fit.

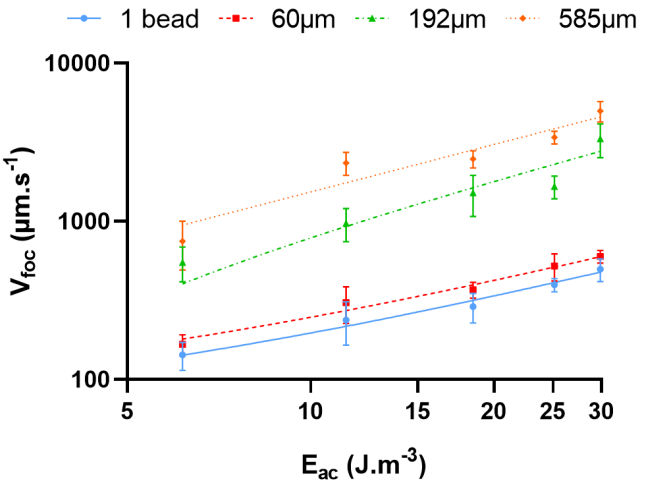

FIG. 7. Focusing velocities of a 60 μm, a 192 μm and a 502 μm diameter aggregates as a function of the acoustic energy. Aggregates are composed of 25 μm polystyrene particles. The focusing velocity of an individual 25 μm polystyrene particle has been added for comparison. The lines are linear fit.

(200 $\mu m.s^{-1}$ for 6 $J.m^{-1}$ and 5 10^3 $\mu m.s^{-1}$ for 30 $J.m^{-1}$).

Finally, the same experiments were performed with particles of 40 μm, as shown in Fig. 8. It is observed that the velocity is slightly increased for an aggregate of 103 μm. A clear, but limited, increase in the focusing velocity is observed for an aggregate of 434 μm. It seems to show that the acceleration by collective effects is limited for larger particles. This observation is confirmed by Fig. 9 where the relative gain in velocity is plotted compared to the case of isolated particles. It shows that the maximum gain (greater than $\times 40$) is obtained for aggregates of small particles (10 μm) and lower acoustic

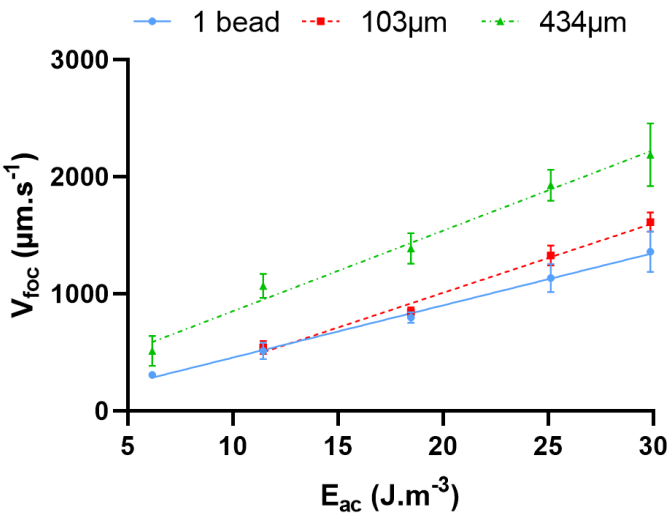

FIG. 8. Focusing velocities of a 103 μm and a 434 μm diameter aggregates depending the acoustic energy. Aggregates are composed of 40 μm polystyrene particles. The focusing velocity of an individual 40 μm polystyrene particle has been added for comparison. The lines are linear fit.

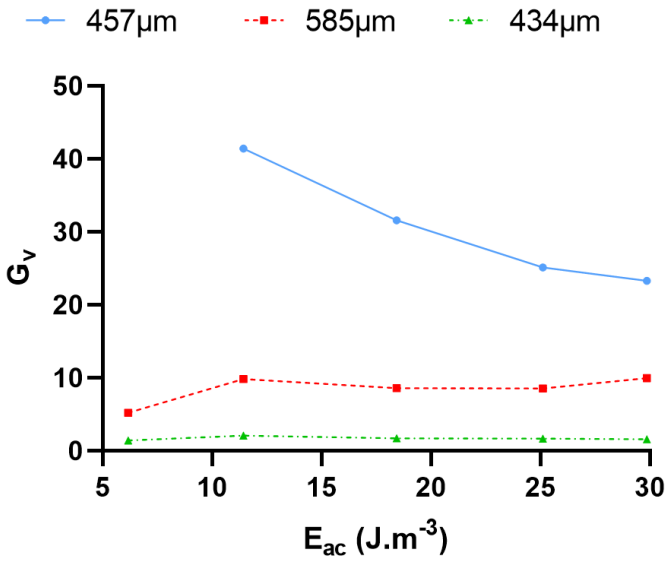

FIG. 9. Relative gain in focusing velocities for the largest aggregates of each particle size depending the acoustic energy. The 457 μm aggregate is made of 10 μm particles, while the 585 μm aggregate is made of 25 μm particles and the 434 μm aggregate is made of 40 μm particles.

It shows that the maximum gain is obtained for aggregates made of 10 μm particles.

energy. Aggregates of 25 μm particles lead to an intermediate gain ($\times 10$) while aggregates made of large particles lead to a limited increase in velocities ($\approx \times 2$). It is also interesting to note that the maximum absolute focusing velocity (up to 5 10^3 $\mu m.s^{-1}$ for 30 $J.m^{-1}$)) is obtained for an aggregate of 585 μm made of 25 μm particles.

These results clearly demonstrate the influence of the

size of an aggregate on the focusing velocity of its constituent particles. Major collective effects seem to appear for aggregates larger than 100 μm. This confirms that for a given acoustic energy, the focusing velocity can be drastically increased by collective effects alone. Promoting interactions between particles to form aggregates therefore appears to be a good strategy for accelerating aggregation phenomena without consuming more energy.

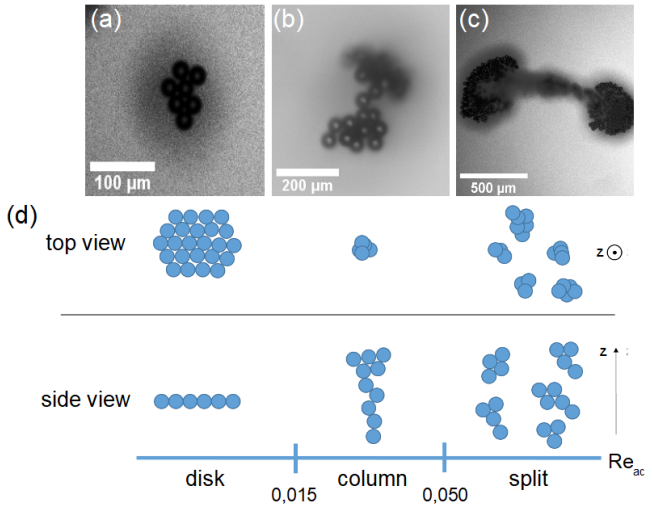

FIG. 10. Different regimes of acoustic focusing observed for an aggregate composed of 25 μm polystyrene particles. Every snapshot has been taken when the aggregate reaches the focusing plane. a) The first regime corresponds to an acoustic focusing where the aggregate keeps its "discoid" initial shape. b) when the acoustic focusing Reynolds number is increased, the aggregate no longer keeps its discoid shape and moves as a column of particles. c) Finally, the aggregate splits into multiple parts for the larger the Re_{ac}. d) The different regimes of aggregates acoustic focusing are summarized as a function of the acoustic focusing Reynolds number. Sketches of the aggregates spatial organizations are presented with top and side views. Three regimes can be distinguished: first, a migration of the all aggregate keeping its spatial organization, for $Re_{ac} \leq 0.015$, then a dislocation of the discoidal aggregate into a column of particles, for $0.015 \leq Re_{ac} \leq 0.050$ and finally a splitting of the aggregate into smaller aggregates for $Re_{ac} \geq 0.050$. Movies on line.

2. *Regimes for the acoustic focusing of aggregates*

The previous results demonstrated that the acoustic focusing of aggregates can be much faster than the focusing of a single isolated particle. It also showed that the larger the aggregate, the higher the focusing velocity.

A closer observation of time series showing the displacement of the aggregate from the bottom of the cavity toward the acoustic levitation plane reveals different behaviors. Indeed, some aggregates keep their original discoid shape, while others are clearly modified in the process in a manner similar to the ones observed for the sedimentation. In the following we classify the various observations into regimes depending on the new parameter introduced previously: the acoustic focusing Reynolds number. The main results are shown in Fig. 10.

First, for $Re_{ac} \leq 0.015$ the aggregate migrates toward the pressure node keeping its disk shape in the (x,y) plane. This observation is true for small aggregates ($D_{ag} \leq 100$ μm) made of small particles ($d_p \leq 40$ μm) and for acoustic energy density ranging from 7 $J.m^{-3}$ to 80 $J.m^{-3}$.

For $0.015 \leq Re_{ac} \leq 0.05$, the discoidal aggregates are affected by a deformation during their focusings. The particles migrate as a column. Once in the levitation plane, particles reorganize themselves and form an aggregate again with an ellipsoidal shape. Typical diameters are around 100 μm.

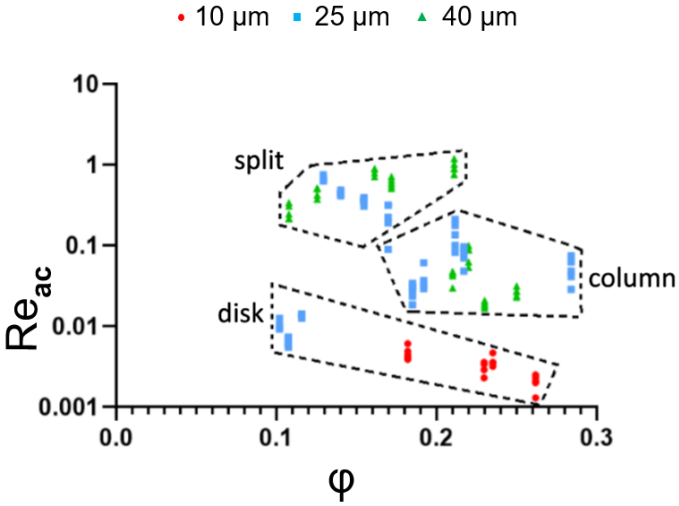

FIG. 11. Acoustic focusing Reynolds number as a function of the aggregate porosity. For low Reynolds numbers aggregates move toward the levitation plane keeping their discoidal shape, especially for small particles (10 μm). For larger particles (25 μm), smaller porosity helps keeping the aggregate as a disk. Increasing Re_{ac} leads first to columns formation then to splitting the columns into smaller aggregates, especially for lower porosities ($0.1 \leq \varphi \leq 0.2$).

Finally, for $Re_{ac} \geq 0.05$, the aggregate fragments into several pieces, each piece being composed of several particles, before reforming in the levitation plane under the effect of the radial component of the acoustic force. In this case, the diameters of the aggregates are ranging between 100 μm up to 500 μm. The relatively large size of the aggregates implies that at a given axial position z the particles do not experience the same acoustic energy density, depending on their position in the aggregate. This can therefore result in an increasing distance between the particles and consequently a breakup of the aggregate into multiple "fragments". This behavior is also comparable to the breakup of particles cloud observed during sedimentation [55]. The particles aggregates would separate in the same way before the radial component of the

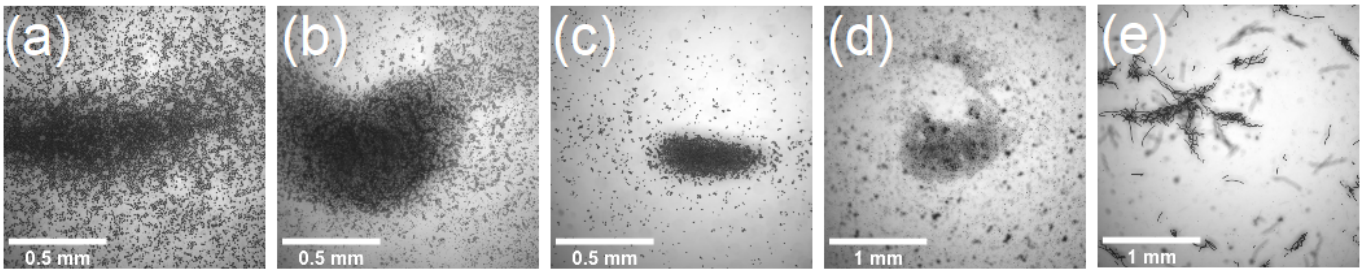

FIG. 12. Formation of aggregates of various microalgae in acoustic levitation after 30 s. a) *Tetraselmis suecica* b) *Nannochloropsis oculata*, c) *Scenedesmus obliquus*, d) *Chlorella vulgaris* and e) *Spirulina platensis*.

acoustic force would force the small aggregates to finally gather in the levitation plane.

It is important to point out that some aggregates, smaller or larger than 100 μm, can migrate toward the levitation plane in the form of columns. It all depends on the speed at which these aggregates migrate. Smaller focusing velocities will delay the transition from one regime to the next, while higher focusing velocities will anticipate it.

We took into account the different sizes of the aggregates. Nevertheless the aggregates are composed of particles of different sizes which lead to various porosities. Consequently we also studied the impact of porosity on focusing dynamics. Optimal configuration for a disk of particles stacked on a surface is $A_{sol-max} = 0.9069$ while minimal porosity of an aggregate is $A_{pores-min} = 0.0931$. Porosity of each aggregate was measured in the focusing plane, just after their formation and before their sedimentation. The results are shown in Fig. 11 as a phase diagram. We distinguish three different regimes for the acoustic focusing of aggregates:

- The first regime corresponds to low acoustic focusing Reynolds numbers ($Re_{ac} \leq 0.015$) which is wide in the diagram. It corresponds to aggregates which migrate with a cohesive disk shape. We have big variations of porosity for this regime from $\varphi = 0.1075$ until $\varphi = 0.2617$. We also notice that all the aggregates made of small particles (10 μm) keep their discoid shape.

- The second regime, for $0.015 \leq Re_{ac} \leq 0.050$, is characterized by a high porosity being $0.185 \leq \varphi \leq 0.284$. In this configuration the aggregate migrates like a column shape.

- Finally the third regime, for $Re_{ac} \geq 0.050$, corresponds to a split of the aggregate. Porosity is lower than the second regime (between $\varphi = 0.1078$ and $\varphi = 0.211$).

We note a tiny frontier between the second and third regimes. That is a fact we observed during our experiments. In the same conditions, at a given acoustic energy density, an aggregate can migrate like a column sometimes and then the second time split into two parts, indicating a transition in the phase diagram. We observe a big variation of porosity for aggregates focusing like a disk shape but only if the acoustic focusing Reynolds number is lower than $Re_{ac} \leq 0.02$. We note a high porosity and medium Re_{ac} for aggregates migrating in a column shape. Finally, for high Re_{ac} and a porosity between $0.1078 \leq \varphi \leq 0.211$, aggregates split in multiple parts.

C. Formation of aggregates of microalgae

We have shown with particles that ARF-induced aggregation can be strongly accelerated if the particles can interact or form small clusters. The next step is then to evaluate whether this phenomenon can be applied to microalgae. Five different microalgae were tested inside the acoustofluidic cavity: *Tetraselmis suecica*, *Nannochloropsis oculata*, *Scenedesmus obliquus*, *Chlorella vulgaris* and *Spirulina platensis*. Their properties are summarized in Tab. I. It can be seen that the sizes (from 1 to 300 μm) and the shapes (circular, ellipsoid, long and wavy) are very different. Fig. 12 shows that, despite very different sizes and properties, all microalgae can be moved by ARF and form aggregates. These aggregates, unlike those of particles, do not generally form a disk shape. The particles, once in the aggregate, have the ability to reorganize themselves to form a disk shape by rolling over each other. Microalgae do not reorganize in the aggregate, which takes on various shapes depending on the side of the (x,y) plane from which they come. In the following, we will focus on the microalga *Scenedesmus*, which has a simple shape, is not too large and has good properties for biofuel production. Moreover, its size is in the range where collective effects are maximum with particles.

It should be noted here that the expression of the ARF given in Eq. 2 is not valid for an ellipsoidal object. More refined models should be used, as the ones proposed by Marston et al. [59], Mitri [60], Silva & Drinkwater [61] or Leao et al. [62]. Some peculiar phenomena can also be observed for elongated metallic nanorods, like self-propulsion [63, 64]. Such behaviors were not observed with microalgae, due to their much lower density. Nevertheless, in the following only collective effects will be discussed, independently of the shape of the microalgae.

	Shape	Size (μm)	Medium	ϕ
Chlorella vulgaris	ellipsoidal	5	non saline	N/A
Scenedesmus obliquus	ellipsoidal	10	non saline	N/A
Spirulina platensis	long / wavy	70-300	non saline	N/A
Nannochloropsis oculata	spherical	1	saline	0.05
Tetraselmis suecica	spherical	20	saline	N/A

TABLE I. Main properties of the five tested microalgae. In general, the acoustic contrast factor ϕ is unknown, except for the *Nannochloropsis* [65] measurement.

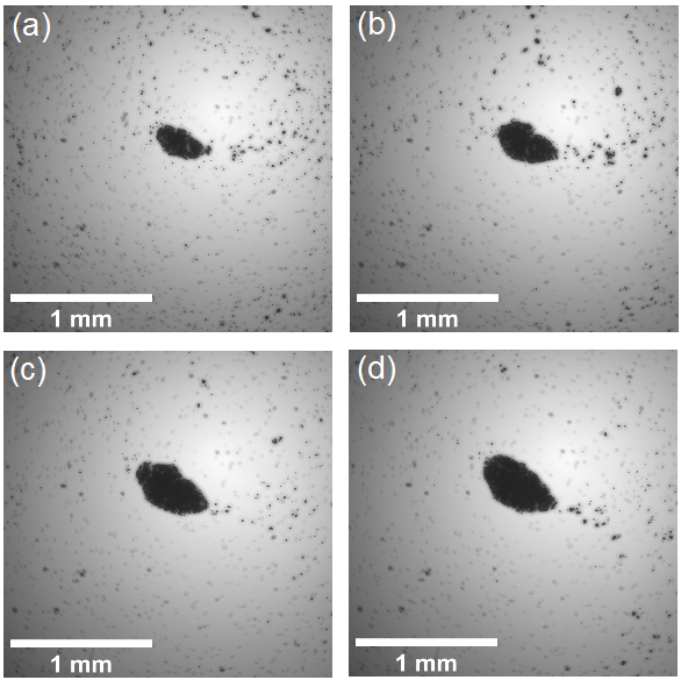

FIG. 13. Time evolution of a *Scenedesmus* aggregate under acoustic depending time: a) 30 s, b) 1 min, c) 3 min, and d) 5 min. Acoustic power is 0.5 W. This aggregate corresponds to the red curve in Fig. 14.

1. *Influence of the acoustic power*

The first step is to study the temporal evolution of an aggregate of *Scenedesmus*, as illustrated in Fig. 13, for a given concentration (395 000 $algae.mm^{-2}$) and a given acoustic power (0.5 W). We note that the position of the aggregate remains the same over time, but that its surface increases regularly as the algae arrive in the support plane.

The influence of acoustic power on aggregation dynamics is also illustrated in Fig. 14a), where snapshots of *Scenedesmus* aggregates obtained after 30 s for increasing acoustic power (from 0.5 W to 1.04 W) are presented. The increase in the aggregate surface area can be clearly seen when the acoustic power is increased.

To quantify these evolutions, the time series of snapshots are post-processed using ImageJ software to measure the area of the aggregate as a function of time. The results are presented in Fig. 14b) where the area of the aggregates is plotted as a function of time over 5 min for 5 different acoustic powers and for a given concentration (395 000 $algae.mm^{-2}$).

The first observation is that the aggregates grow faster when the acoustic power is increased (for a similar given time). After 30 s the aggregate obtained with 0.5 W has an area of 0.06 mm^2, while the aggregate obtained with 1.04 W has an area of 0.17 mm^2. The area of the aggregate is multiplied by a factor of 2.8 when the acoustic power is multiplied by a factor of 2.08.

The second observation is the overall evolution of the aggregate area, which can be separated into two main regimes. The first regime corresponds to short times (up to 50 s). The growth of the aggregates is very fast because all the microalgae that are close to the pressure node are quickly trapped inside the levitation plane. The second regime corresponds to the capture of microalgae further from the levitation plane. It can take a few hundred seconds to finally collect all the microalgae present in the suspension, which corresponds to the slow evolution towards the final asymptotic area of the aggregate. If we apply acoustics a sufficiently long time, the curves should overlap by reaching an asymptotic regime close to the same value. However, for small acoustic powers, there are loss of microalgae. Indeed, for lower powers, part of the algae will have time to sediment toward the bottom of the cavity, resulting in an asymptotic value lower than the one for higher acoustic power.

2. *Influence of the concentration of microalgae*

It has been shown that particle interactions and the creation of small aggregates can lead to a strong increase in the acoustic focusing speed of the aggregates. This suggests that the concentration of particles or microalgae can also play a role in the dynamics of acoustic trapping. For this reason, experiments with different initial concentrations of microalgae have been performed.

The first result is presented in Fig. 15a. It shows microalgae aggregates 30 s after the acoustics were turned on, for 4 different initial concentrations, ranging from 790 000 $algae.mm^{-2}$ (C_1) to 100 000 $algae.mm^{-2}$ (C_4) and for a given acoustic power of 0.90 W. It shows a clear decrease in the surface area of the aggregate when the initial concentration is decreased.

Fig. 15b shows the temporal evolution of the area of the aggregates for the 4 different initial concentrations. The same type of evolution is observed, with a strong growth during the first tens of seconds, followed by a slow evolution towards an asymptotic value. The higher the initial concentration, the faster the aggregation and

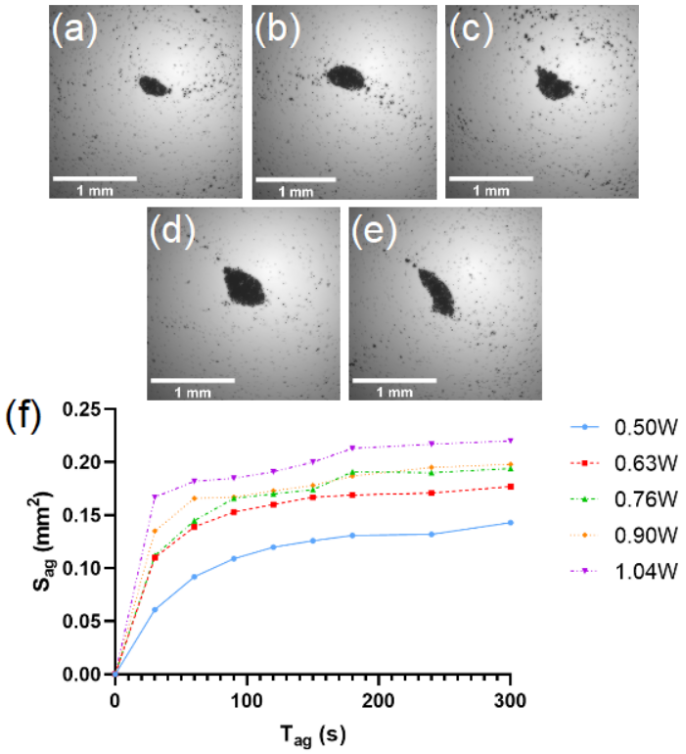

FIG. 14. Aggregate of *Scenedesmus* after 30 s for 5 different acoustic powers: a) 0.5 W, b) 0.63 W, c) 0.76 W, d) 0.90 W and e) 1.04 W. The same concentration is 395 000 $algae.mm^{-2}$. Magnification is 4 X. f) Time evolution of the aggregates area as a function of time for five different acoustic powers.

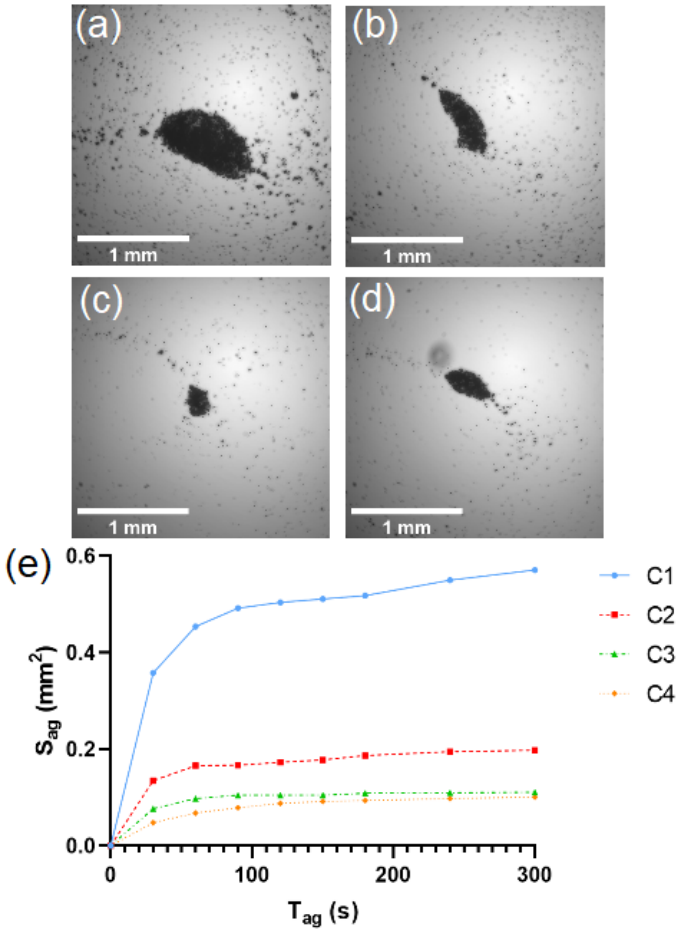

FIG. 15. Evolution of *Scenedesmus* aggregates after 30 s under acoustic. 4 concentrations were used from a) C_1 =790 000 $algae.mm^{-2}$ b) C_2 =395 000 $algae.mm^{-2}$ c) C_3 =200 000 $algae.mm^{-2}$ and d) C_4 =100 000 $algae.mm^{-2}$. Constant acoustic power of 0.9 W was applied. Observation is at 4 X magnification. e) Time evolution of the surface of the aggregates depending on the initial concentration during 5 min under acoutics.

the larger the final area of the aggregate.

It can be assumed that two effects are at play for short times: collective effects as well as the increase in the number of microalgae in the region of the acoustic pressure node. Indeed, the concentration of microalgae is increased by a factor of 2 from C_4 to C_1 but a clear acceleration and increase in the asymptotic surface can be observed from C_2 to C_1 (Fig. 16). This effect is not observed for lower concentrations, which can be explained by a critical concentration beyond which collective effects take place.

For long times, it can be assumed that the final area of the aggregate is directly related to an increasing number of microalgae in the suspension.

D. Multinode cavities and application to microalgae harvesting

It has been shown in the previous section that microalgae behave in a similar way to solid particles. Experiments performed with *Scenedesmus obliquus* show an accelerated formation of flocs when the concentration or power is increased. To extend and further demonstrate the scaling possibilities, a multinode cavity was designed in Poly-DimethylSiloxane (PDMS), as shown in Fig. 17. The device is characterized by a high aspect ratio: the height of the cavity is now $h = 8$ cm, which leads to the creation of 180 levitation planes. A DinoLite™ digital microscope is placed on one side of the rectangular cavity, backlit by a planar white light source, in order to record lateral views of the algae movements under acoustics. Both the transducer and the camera are controlled by a computer (Fig. 17).

A typical example of microalgae aggregation in the multinodal cavity is shown in Fig. 18 for *Tetraselmis suecica* for a given power (1.04 W) and a given concentration. C_0 corresponds to the concentration of the original sample ($C_0 \approx 1\ 10^6$ $algae.mL^{-1}$) provided by the supplier (Teramer®). The sample is then diluted and the result is expressed as the dilution rate of the initial concentration. Fig. 18 illustrates the methodology used to quantify the dynamics of microalgae layer formation in

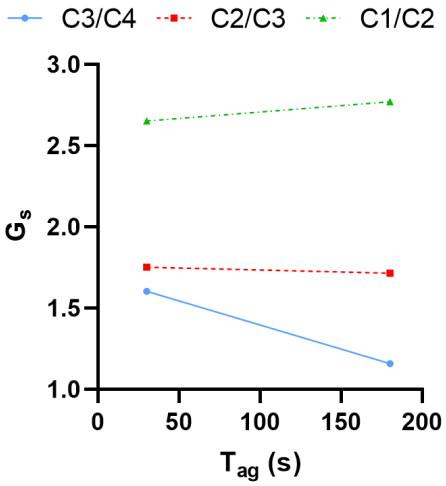

FIG. 16. Relative gain in the size of the aggregates for increasing concentration: from C_4 to C_3, from C_3 to C_2 and from C_2 to C_1. The maximum gain is obtained for the larger concentrations.

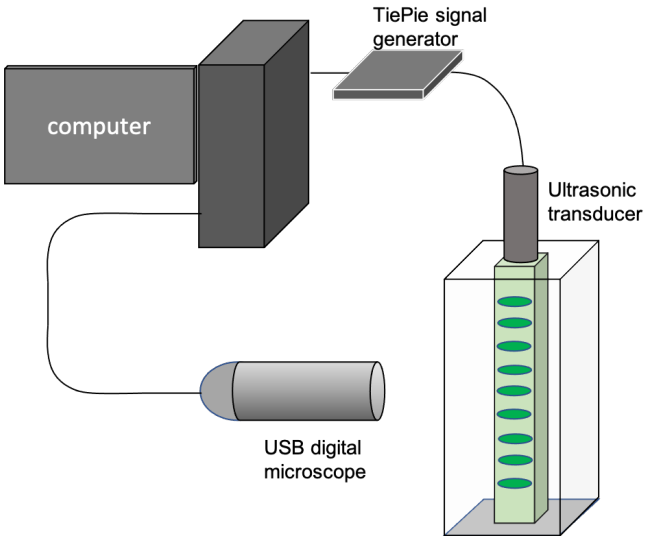

FIG. 17. Sketch of the multinodes system. A 2 MHz transducer is placed at the top of a 8 cm high PDMS resonator with 1x1cm^2 section. The transducer is tuned with a signal generator controlled by a computer. The transducer can be moved inside the cavity allowing variations of height. A DinoLite™ USB microscope camera is located on the side of the resonator. In this study, 180 acoustic nodes were created along the height of the cavity.

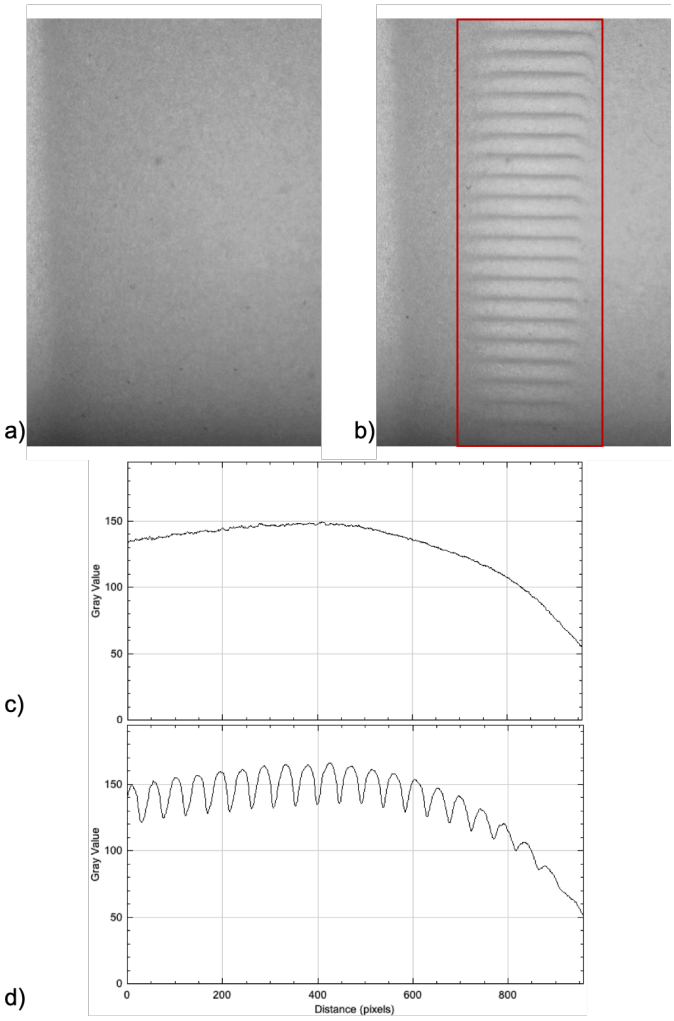

FIG. 18. Illustration of the formation of Tetraselmis algae layers in a multi-node cavity. a) The suspension is initially homogeneously distributed in the volume. b) Once the acoustics are activated, and after a certain time, microalgae layers form at all pressure nodes. To measure the time required for the onset of layer formation, the vertical intensity profile, averaged over a given ROI (red rectangle in b)) is calculated at each time step. c) The profiles are initially smooth, d) before exhibiting an axial modulation after some time under acoustics.

acoustic levitation. Fig. 18a shows the suspension of microalgae homogeneously distributed in the cavity, while Fig. 18b shows several layers of microalgae formed at each pressure node. The red rectangle on each image defines the ROI (Region Of Interest) on which the spatial average intensity profiles were calculated. Figs. 18c,d show the intensity profiles corresponding to Fig. 18a and Fig. 18b, respectively. It can be seen that the intensity profile is initially smooth with an axial variation related to the optical source used to illuminate the cavity. Once the acoustics are activated, microalgae layers are formed, leading to a clear axial modulation of the intensity profile. It is then possible to evaluate the acoustic focusing time T_{flocs} corresponding to the first spatial modulation of the intensity profile. We apply a Fast Fourier Transform (FFT) on the intensity profile. For a smooth profile, no peak is observed in the FFT spectrum. On the contrary, a clear axial modulation leads to many peaks in the FFT. The time during which a clear peak appears in the FFT is the criterion used to define the appearance of the first spatial modulation and therefore T_{flocs}. Using this principle, the acoustic focusing time T_{flocs} was

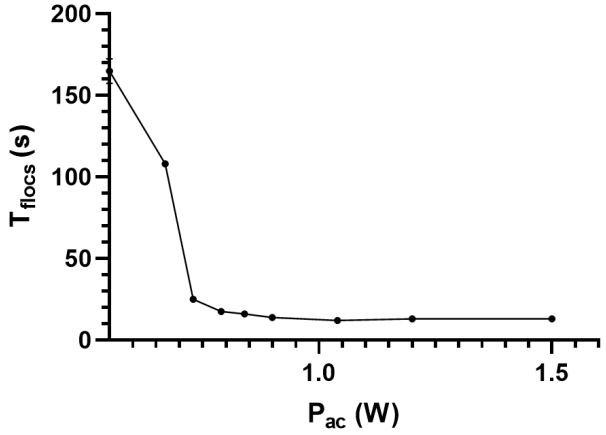

FIG. 19. Evolution of the focusing time as a function of the acoustic power P_{ac} for a given concentration ($\frac{C_0}{2}$). One can see that increasing the power above 0.5 W leads to no acceleration of the acoustic aggregation of the microalgae.

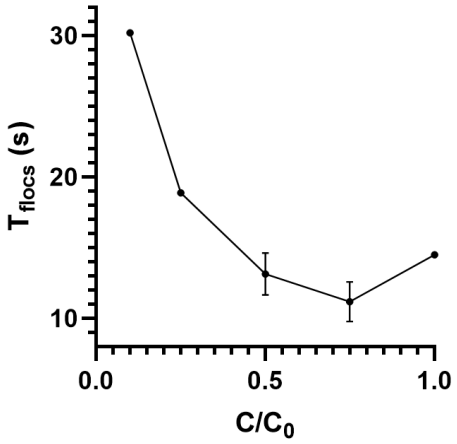

FIG. 20. Evolution of the focusing time as a function of the concentration for a given amplitude of the acoustic force. One can see that the concentration can be optimized to accelerate the formation of aggregates of microalgae with no increase of the energy used by the system ($P_{ac} = 1.2\ W$).

measured for a given concentration ($\frac{C_0}{2}$) as a function of the acoustic power. The result is presented in Fig. 19. It can be seen that the formation of microalgae layers is strongly accelerated up to 0.5 W. For higher acoustic powers, there is no net gain in the dynamics of layer formation.

Using the same principle, the acoustic focusing time was measured for five different concentrations that were different dilutions of the initial suspension with concentration C_0. The result is shown in Fig. 20. It can be clearly seen that the focusing time is indeed greatly reduced, i.e. aggregation is accelerated, simply by increasing the concentration of the suspension. Interestingly, it can also be seen that the concentration should not be too high. A plateau is observed for the highest concentration and even an increase in the time needed to start forming layers can be observed for the highest concentration, suggesting that other effects, such as screening effects, are at play for higher concentrations.

These results can be exploited in the following way. The multi-node static resonator can be further improved and integrated into modular processes, between the growth and post-processing stages. The residence time can be defined as the energy efficiency parameter, determining the energy consumption of the harvester and the efficiency of the whole process. The residence time can be controlled either by the acoustic power or by the initial concentration at the inlet of the harvesting unit, which can be obtained either naturally in the growth process or by a complementary preconcentration method. For example, a typical biomass-to-biocrude process relies on cultivation in a raceway or tubular reactor, with subsequent harvesting by filtration before entering a hydrothermal liquefaction (HTL) unit. The harvesting step is critical to determine the energy efficiency of the process, with a concentration factor higher than 100 $\times$. Such a requirement consumes a lot of energy per filtration unit, not to mention its maintenance costs.

The modularity of the process allows to complement an existing harvesting method with a static ultrasonic cavity. This will allow to lower the target concentration of the filtration unit, corresponding to the critical concentration needed to trigger the accelerated acoustic focusing. This should reduce the energy consumption of the existing unit, as well as the residence time of the acoustic collector. This approach is advantageous compared to the more common ultrasonic flow channels associated with ultrasonic harvesting in the literature [66]. The scaling of flow cells is associated with substantial energy costs, due to the co-competition between the flow and acoustic focusing time scales, a problem that is solved by the use of a static resonator.

A possible integration and a 4-step protocol for such a static ultrasonic accelerated collector is presented in Fig. 21a,b,c,d. Figs 21e,f illustrate Fig. 21b and Fig. 21c, respectively. Fig. 21e shows the formation of multiple layers of microalgae, which can be obtained quickly (a few seconds), while Fig. 21f shows the formation of large aggregates, or flakes, which sediment quickly and can then be harvested as illustrated in Fig. 21d.

VI. CONCLUSION

The efficiency of microalgae collection is essential in the biofuel exploitation process. The main current challenges are high energy consumption and cost. Acoustophoresis is a promising technology, non-intrusive, contactless and without added product. The second advantage is its low energy consumption. Therefore, two parameters that impact the dynamics of aggregate formation have been studied. The first is the acoustic power. By increasing the acoustic power, the ARF also increases.

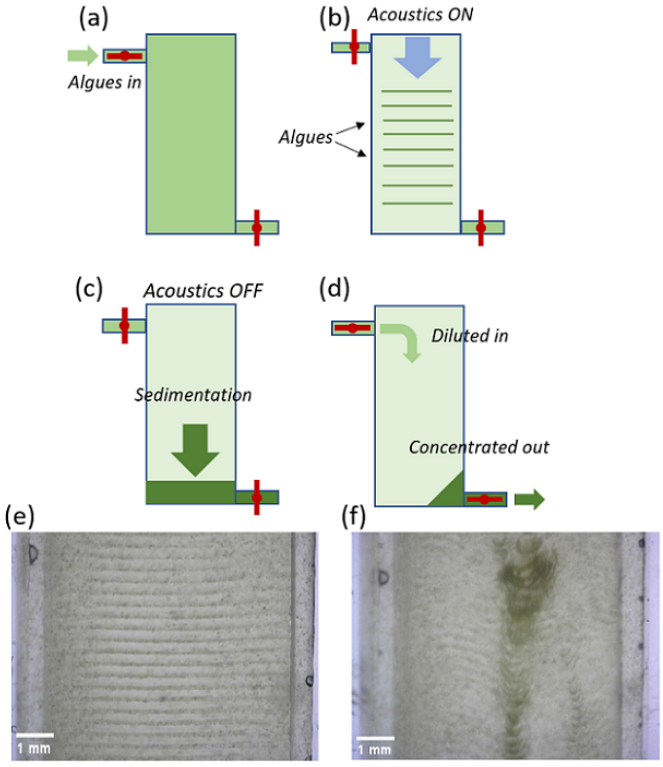

FIG. 21. Schematic of the harvesting process, including the static settler/harvester. The process works in four steps: the diluted solution enters the tank after growth, e.g. from the circulation channel, or after preconcentration (a); the acoustic field is applied for several minutes (b); the acoustics are switched off, resulting in sedimentation (c) and a new solution is introduced into the tank, displacing the concentrate into the post-treatment unit, e.g. HTL (d). Side views showing the formation of several layers of microalgae (e) followed by the formation of large clusters that rapidly sediment in the middle of the cavity (f). Movies online.

Therefore, the particles or microalgae move faster towards the levitation plane. The transverse component of the ARF is also increased which leads to rapid aggregation of microalgae. Increasing the acoustic power leads to higher energy consumption. However, there is also an optimal power beyond which acoustic aggregation is no longer accelerated. Another option is to exploit a second parameter which is the concentration. Indeed, increasing the concentration leads to collective effects.

This study showed that particles close to each other interact with each other. This leads to a strong acceleration of particle groups that thus reach the levitation plane much faster than isolated particles, without increasing the acoustic power. Another consequence of collective effects is the formation of small aggregates. Acoustically, an aggregate cannot be described as several individual particles but rather as a new object. The migration dynamics is strongly accelerated (up to $\times$ 20) for larger aggregates compared to an isolated particle for the same energy consumption.

Collective motions can be complex, depending on the acoustic focusing speed. Three regimes (disk, column, split) were identified, according to an acoustic focusing Reynolds number. The porosity of the aggregates was also analyzed with the three dynamic focusing regimes, showing a lower average porosity for the split regime and a higher average porosity for the column regime.

A multi-node cavity was used to evaluate the influence of suspension concentration on microalgae (*Tetraselmis*) aggregation dynamics in acoustic pressure nodes. It was shown that, for a given power, increasing the concentration leads to a clear acceleration of microalgae layer formation at acoustic pressure nodes. It also appears that aggregation is slowed down if the concentration is too high, probably due to a screening effect, suggesting an optimal concentration to minimize acoustic aggregation time, without increasing the energy.

The advantage of the proposed approach is that the geometry can be kept the same and the performance optimized by adjusting the concentration of the manipulated suspension.

Acknowledgements The authors thank TotalEnergies - OneTech R&D for funding the microalgae experiments, M.Questel and C.Desplobins for help with experiments in PERL, F.Monlau for providing algae samples, and A.Lansoy for discussions. The authors also thank Aenitis Technologies for funding the experiments on micro-particles as well as L. Bellebon's PhD thesis, with help of the ANRT (Agence Nationale pour la Recherche Technologique, French National Agency for Technological Research) .

[1] C. Bouyer, P. Chen, S. Güven, T. T. Demirtaş, T. J. Nieland, F. Padilla, and U. Demirci, A bio-acoustic levitational (bal) assembly method for engineering of multilayered, 3d brain-like constructs, using human embryonic stem cell derived neuro-progenitors, Advanced materials **28**, 161 (2016).

[2] Z. Ma, A. W. Holle, K. Melde, T. Qiu, K. Poeppel, V. M. Kadiri, and P. Fischer, Acoustic holographic cell patterning in a biocompatible hydrogel, Advanced Materials **32**, 1904181 (2020).

[3] K. Olofsson, V. Carannante, M. Ohlin, T. Frisk, K. Kushiro, M. Takai, A. Lundqvist, B. Önfelt, and M. Wiklund, Acoustic formation of multicellular tumor spheroids enabling on-chip functional and structural imaging, Lab on a Chip **18**, 2466 (2018).

[4] N. Jeger-Madiot, L. Arakelian, N. Setterblad, P. Bruneval, M. Hoyos, J. Larghero, and J.-L. Aider, Self-organization and culture of mesenchymal stem cell

spheroids in acoustic levitation, Scientific reports **11**, 1 (2021).
[5] L. Rabiet, L. Arakelian, N. Jeger-Madiot, D. R. García, J. Larghero, and J.-L. Aider, Acoustic levitation as a tool for cell-driven self-organization of human cell spheroids during long-term 3d culture, Biotechnology and Bioengineering **121**, 1421 (2024).
[6] L. Rabiet, N. Jeger-Madiot, D. R. García, L. Tosca, G. Tachdjian, S. Kellouche, R. Agniel, J. Larghero, J.-L. Aider, and L. Arakelian, Improved functionality of hepatic spheroids cultured in acoustic levitation compared to existing 2d and 3d models, Scientific Reports **14**, 21528 (2024).
[7] P.-H. Huang, N. Nama, Z. Mao, P. Li, J. Rufo, Y. Chen, Y. Xie, C.-H. Wei, L. Wang, and T. J. Huang, A reliable and programmable acoustofluidic pump powered by oscillating sharp-edge structures, Lab on a Chip **14**, 4319 (2014).
[8] C. Zhang, X. Guo, P. Brunet, and L. Royon, The effect of sharp-edge acoustic streaming on mixing in a microchannel, in *Annales du Congrès Annuel de la Société Française de Thermique 2020* (2020).
[9] S. J. Brotton and R. I. Kaiser, Controlled chemistry via contactless manipulation and merging of droplets in an acoustic levitator, Analytical Chemistry **92**, 8371 (2020).
[10] J. H. Jung, G. Destgeer, B. Ha, J. Park, and H. J. Sung, On-demand droplet splitting using surface acoustic waves, Lab on a Chip **16**, 3235 (2016).
[11] D. J. Collins, T. Alan, K. Helmerson, and A. Neild, Surface acoustic waves for on-demand production of picoliter droplets and particle encapsulation, Lab on a Chip **13**, 3225 (2013).
[12] I. Lentacker, I. De Cock, R. Deckers, S. De Smedt, and C. Moonen, Understanding ultrasound induced sonoporation: definitions and underlying mechanisms, Advanced drug delivery reviews **72**, 49 (2014).
[13] J. Shi, D. Ahmed, X. Mao, S.-C. S. Lin, A. Lawit, and T. J. Huang, Acoustic tweezers: patterning cells and microparticles using standing surface acoustic waves (ssaw), Lab on a Chip **9**, 2890 (2009).
[14] A. Lenshof, C. Magnusson, and T. Laurell, Acoustofluidics 8: Applications of acoustophoresis in continuous flow microsystems, Lab on a Chip **12**, 1210 (2012).
[15] P. Sajeesh and A. K. Sen, Particle separation and sorting in microfluidic devices: a review, Microfluidics and nanofluidics **17**, 1 (2014).
[16] F. Lickert, M. Ohlin, H. Bruus, and P. Ohlsson, Acoustophoresis in polymer-based microfluidic devices: Modeling and experimental validation, The Journal of the Acoustical Society of America **149**, 4281 (2021).
[17] M. Wu, Z. Mao, K. Chen, H. Bachman, Y. Chen, J. Rufo, L. Ren, P. Li, L. Wang, and T. J. Huang, Acoustic separation of nanoparticles in continuous flow, Advanced functional materials **27**, 1606039 (2017).
[18] N. R. Skov, P. Sehgal, B. J. Kirby, and H. Bruus, Three-dimensional numerical modeling of surface-acoustic-wave devices: Acoustophoresis of micro-and nanoparticles including streaming, Physical Review Applied **12**, 044028 (2019).
[19] F. Petersson, A. Nilsson, C. Holm, H. Jönsson, and T. Laurell, Separation of lipids from blood utilizing ultrasonic standing waves in microfluidic channels, Analyst **129**, 938 (2004).
[20] A. Urbansky, P. Ohlsson, A. Lenshof, F. Garofalo, S. Scheding, and T. Laurell, Rapid and effective enrichment of mononuclear cells from blood using acoustophoresis, Scientific reports **7**, 17161 (2017).
[21] D. Wu, D. Baresch, C. Cook, Z. Ma, M. Duan, D. Malounda, D. Maresca, M. P. Abundo, J. Lee, S. Shivaei, *et al.*, Biomolecular actuators for genetically selective acoustic manipulation of cells, Science Advances **9**, eadd9186 (2023).
[22] S. Li, X. Ding, Z. Mao, Y. Chen, N. Nama, F. Guo, P. Li, L. Wang, C. E. Cameron, and T. J. Huang, Standing surface acoustic wave (ssaw)-based cell washing, Lab on a Chip **15**, 331 (2015).
[23] H. R. Sugier, L. Bellebon, J.-L. Aider, J. Larghero, J. Peltzer, and C. Martinaud, Feasibility of an acoustophoresis-based system for a high-throughput cell washing: application to bioproduction, Cytotherapy (2023).
[24] R. E. Schwartz, C. F. Hirsch, D. F. Sesin, J. E. Flor, M. Chartrain, R. E. Fromtling, G. H. Harris, M. J. Salvatore, J. M. Liesch, and K. Yudin, Pharmaceuticals from cultured algae, Journal of industrial microbiology and biotechnology **5**, 113 (1990).
[25] J. Ullmann and D. Grimm, Algae and their potential for a future bioeconomy, landless food production, and the socio-economic impact of an algae industry, Organic Agriculture **11**, 261 (2021).
[26] E. W. Becker, Micro-algae as a source of protein, Biotechnology advances **25**, 207 (2007).
[27] S. Ścieszka and E. Klewicka, Algae in food: A general review, Critical reviews in food science and nutrition **59**, 3538 (2019).
[28] H.-M. D. Wang, C.-C. Chen, P. Huynh, and J.-S. Chang, Exploring the potential of using algae in cosmetics, Bioresource technology **184**, 355 (2015).
[29] S. Joshi, R. Kumari, and V. N. Upasani, Applications of algae in cosmetics: An overview, Int. J. Innov. Res. Sci. Eng. Technol **7**, 1269 (2018).
[30] R. Ranjith Kumar, P. Hanumantha Rao, and M. Arumugam, Lipid extraction methods from microalgae: a comprehensive review, Frontiers in Energy Research **2**, 61 (2015).
[31] L. Christenson and R. Sims, Production and harvesting of microalgae for wastewater treatment, biofuels, and bioproducts, Biotechnology advances **29**, 686 (2011).
[32] F. Zhao, H. Chu, Z. Yu, S. Jiang, X. Zhao, X. Zhou, and Y. Zhang, The filtration and fouling performance of membranes with different pore sizes in algae harvesting, Science of the Total Environment **587**, 87 (2017).
[33] Y. Chen, J. Liu, and Y.-H. Ju, Flotation removal of algae from water, Colloids and Surfaces B: Biointerfaces **12**, 49 (1998).
[34] A. J. Dassey and C. S. Theegala, Harvesting economics and strategies using centrifugation for cost effective separation of microalgae cells for biodiesel applications, Bioresource technology **128**, 241 (2013).
[35] Y. S. Najjar and A. Abu-Shamleh, Harvesting of microalgae by centrifugation for biodiesel production: A review, Algal Research **51**, 102046 (2020).
[36] Z. Wu, Y. Zhu, W. Huang, C. Zhang, T. Li, Y. Zhang, and A. Li, Evaluation of flocculation induced by ph increase for harvesting microalgae and reuse of flocculated medium, Bioresource technology **110**, 496 (2012).
[37] C. Wan, M. A. Alam, X.-Q. Zhao, X.-Y. Zhang, S.-L.

Guo, S.-H. Ho, J.-S. Chang, and F.-W. Bai, Current progress and future prospect of microalgal biomass harvest using various flocculation technologies, Bioresource technology **184**, 251 (2015).
[38] S. Salim, N. Kosterink, N. T. Wacka, M. Vermuë, and R. Wijffels, Mechanism behind autoflocculation of unicellular green microalgae ettlia texensis, Journal of biotechnology **174**, 34 (2014).
[39] J. Zhang and B. Hu, A novel method to harvest microalgae via co-culture of filamentous fungi to form cell pellets, Bioresource Technology **114**, 529 (2012).
[40] E. Poelman, N. De Pauw, and B. Jeurissen, Potential of electrolytic flocculation for recovery of micro-algae, Resources, conservation and recycling **19**, 1 (1997).
[41] L. V. King, On the acoustic radiation pressure on spheres, Proceedings of the Royal Society of London. Series A-Mathematical and Physical Sciences **147**, 212 (1934).
[42] K. Yosioka and Y. Kawasima, Acoustic radiation pressure on a compressible sphere, Acustica **5**, 167 (1955).
[43] L. P. Gor'kov, On the forces acting on a small particle in an acoustical field in an ideal fluid, in *Selected Papers of Lev P. Gor'kov* (World Scientific Publishing Co., 2014) pp. 315–317.
[44] H. Bruus, Acoustofluidics 7: The acoustic radiation force on small particles, Lab on a Chip **12**, 1014 (2012).
[45] A. Doinikov, Acoustic radiation pressure on a rigid sphere in a viscous fluid, Proceedings of the Royal Society of London. Series A: Mathematical and Physical Sciences **447**, 447 (1994).
[46] A. A. Doinikov, Acoustic radiation force on a spherical particle in a viscous heat-conducting fluid. ii. force on a rigid sphere, The Journal of the Acoustical Society of America **101**, 722 (1997).
[47] G. Whitworth, M. A. Grundy, and W. T. Coakley, Transport and harvesting of suspended particles using modulated ultrasound, Ultrasonics **29**, 439 (1991).
[48] W. L. Nyborg, Physical principles of ultrasound, Ultrasound : Its Application in Medicine and Biology **1**, 1 (1978).
[49] R. E. Apfel, Acoustic radiation pressure - principles and application to separation science, Fortschritte der akustik , 19 (1990).
[50] G. T. Silva and H. Bruus, Acoustic interaction forces between small particles in an ideal fluid, Physical Review E **90**, 063007 (2014).
[51] J. Leão-Neto, J. Lopes, and G. Silva, Core-shell particles that are unresponsive to acoustic radiation force, Physical Review Applied **6**, 024025 (2016).
[52] O. Dron and J.-L. Aider, Acoustic energy measurement for a standing acoustic wave in a micro-channel, Europhysics Letters **97**, 44011 (2012).
[53] L. Bellebon, H. R. Sugier, J. Larghero, J. Peltzer, C. Martinaud, M. Hoyos, and J.-L. Aider, Characterization of mesenchymal stromal cells physical properties using acoustic radiation force, Frontiers in Physics , 715 (2022).
[54] N. Jeger-Madiot, X. Mousset, C. Dupuis, L. Rabiet, M. Hoyos, J.-M. Peyrin, and J.-L. Aider, Controlling the force and the position of acoustic traps with a tunable acoustofluidic chip: Application to spheroid manipulations, The Journal of the Acoustical Society of America **151**, 4165 (2022).
[55] É. Guazzelli, Sedimentation of small particles: how can such a simple problem be so difficult?, Comptes Rendus Mecanique **334**, 539 (2006).
[56] S. G. Huisman, T. Barois, M. Bourgoin, A. Chouippe, T. Doychev, P. Huck, C. E. B. Morales, M. Uhlmann, and R. Volk, Columnar structure formation of a dilute suspension of settling spherical particles in a quiescent fluid, Physical Review Fluids **1**, 074204 (2016).
[57] M. Uhlmann and T. Doychev, Sedimentation of a dilute suspension of rigid spheres at intermediate galileo numbers: the effect of clustering upon the particle motion, Journal of fluid mechanics **752**, 310 (2014).
[58] T. Doychev, *The dynamics of finite-size settling particles* (KIT Scientific Publishing, 2015).
[59] P. L. Marston, W. Wei, and D. B. Thiessen, Acoustic radiation force on elliptical cylinders and spheroidal objects in low frequency standing waves, in *AIP Conference Proceedings*, Vol. 838 (AIP, 2006) pp. 495–499.
[60] F. Mitri, Acoustic radiation force on oblate and prolate spheroids in bessel beams, Wave Motion **57**, 231 (2015).
[61] G. T. Silva and B. W. Drinkwater, enAcoustic radiation force exerted on a small spheroidal rigid particle by a beam of arbitrary wavefront: Examples of traveling and standing plane waves, The Journal of the Acoustical Society of America **144**, EL453 (2018).
[62] J. P. Leao-Neto, M. Hoyos, J.-L. Aider, and G. T. Silva, Acoustic radiation force and torque on spheroidal particles in an ideal cylindrical chamber, The Journal of the Acoustical Society of America **149**, 285 (2021).
[63] W. Wang, L. A. Castro, M. Hoyos, and T. E. Mallouk, Autonomous motion of metallic microrods propelled by ultrasound, ACS nano **6**, 6122 (2012).
[64] G. Dumy, N. Jeger-Madiot, X. Benoit-Gonin, T. E. Mallouk, M. Hoyos, and J.-L. Aider, Acoustic manipulation of dense nanorods in microgravity, Microgravity Science and Technology **32**, 1159 (2020).
[65] E. H. Gómez, J. Tryner, A. J. Aligata, J. C. Quinn, and A. J. Marchese, Measurement of acoustic properties of microalgae and implications for the performance of ultrasonic harvesting systems, Algal research **31**, 77 (2018).
[66] R. Bosma, W. A. Van Spronsen, J. Tramper, and R. H. Wijffels, Ultrasound, a new separation technique to harvest microalgae, Journal of Applied Phycology **15**, 143 (2003).
[67] F. B. Wijaya and K.-M. Lim, Numerical calculation of acoustic radiation force and torque acting on rigid nonspherical particles, Acta Acustica united with Acustica **101**, 531 (2015).
[68] B. L. Marrone, R. E. Lacey, D. B. Anderson, J. Bonner, J. Coons, T. Dale, C. M. Downes, S. Fernando, C. Fuller, B. Goodall, J. E. Holladay, K. Kadam, D. Kalb, W. Liu, J. B. Mott, Z. Nikolov, K. L. Ogden, R. T. Sayre, B. G. Trewyn, and J. A. Olivares, Review of the harvesting and extraction program within the national alliance for advanced biofuels and bioproducts, Algal Research **33**, 470 (2018).
[69] O. Dron, *Acoustic manipulation of micro-particles. Application to micro*-PIV *measurements.*, Ph.D. thesis, Université Paris 7 - Denis Diderot (2011).